TITLE: Identification of a conserved neutralizing epitope present on spike proteins from all highly pathogenic coronaviruses

SHORT TITLE: Conserved neutralizing coronavirus spike epitope

Yimin Huang[1]†, Annalee W. Nguyen[2]†, Ching-Lin Hsieh[1], Rui Silva[1], Oladimeji S. Olaluwoye[4], Rebecca E. Wilen[2], Tamer S. Kaoud[3], Laura R. Azouz[2], Ahlam N. Qerqez[2], Kevin C. Le[2], Amanda L. Bohanon[1], Andrea M. DiVenere[2], Yutong Liu[2], Alison G. Lee[1], Dzifa Amengor[1], Kevin N. Dalby[3], Sheena D'Arcy[4], Jason S. McLellan[1,5], Jennifer A. Maynard[2,5]*

†These authors contributed equally to this work. [1]Department of Molecular Biosciences, The University of Texas, Austin, TX 78712, USA. [2]Department of Chemical Engineering, The University of Texas, Austin, TX 78712, USA. [3]Division of Chemical Biology and Medicinal Chemistry, The University of Texas, Austin, TX 78712, USA. [4]Department of Chemistry and Biochemistry, The University of Texas, Dallas, TX 75080, USA. [5]LaMontagne Center for Infectious Diseases, The University of Texas, Austin, TX 78712, USA. *Corresponding author.

ABSTRACT

Three pathogenic human coronaviruses have emerged, with SARS-CoV-2 causing a global pandemic. While therapeutic antibodies targeting the SARS-2 spike currently focus on the poorly conserved receptor-binding domain, targeting essential neutralizing epitopes on the more conserved S2 domain may provide broader protection. We report three antibodies, binding epitopes conserved on the pre-fusion MERS, SARS-1 and SARS-2 spike S2 domains. Antibody 3A3 binds a conformational epitope with ~2.5 nM affinity and neutralizes in *in vitro* SARS-2 cell fusion and pseudovirus assays. Hydrogen-deuterium exchange mass spectrometry identified residues 980-1006 in the flexible hinge region at the S2 apex as the 3A3 epitope, consistent with binding to natural and engineered spike variants. This location at the spike trimer interface suggests 3A3 prevents the S2 conformational rearrangements required for virus-host cell fusion. This work defines a highly conserved vulnerable site on the SARS-2 S2 domain and may help guide the design of pan-protective spike immunogens.

TEASER

A conserved, neutralizing epitope in the S2 domain of coronavirus spike was identified as a target for pan-coronavirus therapy and vaccination.

INTRODUCTION

COVID-19, the disease caused by severe acute respiratory syndrome coronavirus 2 (SARS-2), has been responsible for over 2 million deaths worldwide since it was identified in late 2019. This pandemic is the latest and largest of three deadly coronavirus outbreaks, including those caused by SARS-CoV-1 (SARS-1) in 2002 and Middle Eastern Respiratory Syndrome coronavirus (MERS) in 2012. Although COVID-19 has a case fatality rate estimated at ~1-3% versus ~15% for SARS-1 and ~34% for MERS (*1*), it has proven to be far more infectious and its spread has impacted every aspect of society worldwide. Four other coronaviruses are known to infect humans, resulting in relatively mild upper respiratory disease and symptoms: 229E, OC43 (both discovered in the 1960s), NL63 (2004), and HKU1 (2005). All seven of these coronaviruses are zoonotic and a large number of other coronaviruses are endemic in animals, foreshadowing future coronavirus outbreaks.

Coronaviruses are enveloped positive sense, single-stranded RNA viruses that invade target cells by fusion of the viral envelope with the target cell membrane, mediated by the spike glycoprotein. The spike is a homo-trimer comprised of the S1 and S2 domains, with S2 proximal to the viral envelope forming a stalk-like structure and S1 forming a cap over the end of S2. Each S1 domain monomer contains an N-terminal domain (NTD) and a receptor-binding domain (RBD) that overlaps adjacent NTDs and RBDs within the trimer, forming a responsive surface that allows each RBD to extend to the "up" position for receptor binding or tuck into the "down" position for immune shielding. When all three RBDs engage a receptor in the up position and target-cell-anchored proteases prime the spike, the S1 domain is released from S2, propelling the fusion peptide into the target cell surface. Simultaneously, S2 undergoes a massive structural rearrangement to bring the viral envelope into contact with the target cell, initiating fusion and leaving spike in the post-fusion state (*2*).

A powerful strategy to prevent coronavirus fusion is to disrupt the interaction between the RBD and its host cell receptor. For SARS-2, the receptor is angiotensin-converting enzyme 2 (ACE2), and antibodies that block RBD binding to ACE2 are potently neutralizing and common in convalescent patient serum (*3*). Accordingly, most monoclonal antibody therapies in development target this interaction (*4*). However, RBD sequences from different coronaviruses are quite different to allow for binding to various host cell receptors. Even within the three human-relevant coronaviruses that bind ACE2 (SARS-1, SARS-2 and NL63), RBD-binding antibodies exhibit limited cross-reactivity (*5*), consistent with the low level of S1 sequence conservation (~20-24% identity, ~41-52% similarity; fig. S1). As a result, it has been difficult to identify antibodies binding multiple lineage B β-coronaviruses, such as SARS-1 and SARS-2 (*6*), much less across lineages, such as the lineage C MERS.

By contrast, the spike S2 domain is the most conserved spike domain, with 63-98% sequence similarity in pairwise comparisons across the seven human coronaviruses (fig. S1). Moreover, the analogous domain in influenza, respiratory syncytial virus (RSV) and HIV contains potently neutralizing epitopes (*7, 8*), prompting speculation that the spike S2 domain may also serve as an effective target for neutralizing antibodies. Multiple potential mechanisms inhibit viral fusion by targeting the S2 domain, including preventing S2 conformational rearrangement, blocking the fusion peptide (*9-11*), and interfering with S2 proteolytic processing (*12*), or inducing premature S1 shedding and non-productive transformation into the post-fusion spike. However, few antibodies binding the S2 domain of SARS-2 or conserved epitopes on S2 have yet been reported in detail.

Here, we aimed to identify antibodies binding epitopes conserved across all known highly pathogenic coronavirus strains. To focus immune responses on the S2 domain, we immunized mice with a stabilized MERS S2 protein and isolated antibodies using alternate rounds of selection with the MERS S2 and intact SARS-2 spike using phage display. Of three high affinity, cross-reactive antibodies characterized, 3A3 neutralizes SARS-2 spike in cell fusion and pseudovirus assays by binding a conformational epitope at the apex of the S2 domain. This epitope is only accessible when the RBDs shift to the up position and becomes increasingly accessible to 3A3 in spike variants that stabilize the RBD-up conformation, a feature which correlates with increased viral transmission. The 3A3 epitope defines a novel site of vulnerability on spike, which is increasingly relevant for the more transmissible spike variants and may be an important target for future pan-coronavirus vaccines and therapeutic strategies.

RESULTS

Isolation of antibodies binding the S2 domain of SARS-1, SARS-2 and MERS spikes

To generate S2-specific antibodies, three Balb/c mice were immunized with stabilized MERS S2 protein and boosted four weeks later, resulting in a robust serum antibody with titers >10,000. The MERS S2 protein includes amino acid residues 763-1291 of MERS-S-2P of the MERS spike protein with a c-terminal T4 phage fibritin (foldon) domain that assembles into a pre-fusion trimer. To generate immune antibody libraries, total mRNA was isolated from the mouse spleens and reverse transcribed; the antibody variable regions were then amplified (*13*) and inserted into the pMopac24 M13 bacteriophage display vector (*14*) for the expression of pIII-scFv-c-myc tag fusion proteins. The phage display library (~3.1×10^8 individual clones) was subjected to four rounds of panning with immobilized antigen: anti-c-myc antibody to deplete truncated non-expressing clones, then MERS S2, and finally SARS-2 spike at a high followed by moderate coating concentrations. These experiments used stabilized spike 2P with prolines at residues 986 and 987 (*15*); in this work, "spike" refers to the extracellular domains from SARS-1, SARS-2, MERS, and HKU1 containing the homologous 2P mutations fused to a foldon domain unless otherwise noted.

Phage clones isolated after rounds 3 and 4 were confirmed to bind MERS S2 and SARS-2 spike by ELISA and evaluated for binding to uncoated plates and the foldon domain. While no clones exhibited plate or milk binding, ~85% of round 3 and 4 clones bound the shared foldon domain fused to the RSV F protein (*16*)(**Fig S2**). One of these foldon binders, 3E11, was carried forward as a control antibody. Three unique clone families were identified from the remaining clones specific to the spike protein: 3A3, 4A5, and 4H2. Antibody 3A3 and close relatives appeared in round 3 and were enriched to ~10% of the population after round 4, while 4A5 and 4H2 were unique sequences isolated after round 4 of panning.

Cross-reactive antibodies bind the spike S2 domain with high affinity and specificity

After expression in ExpiCHO cells and purification of 3A3, 4A5, 4H2, and 3E11 as full-length antibodies with human Fc and kappa domains, the antibodies were biophysically characterized to measure spike binding affinity by biolayer interferometry, thermal unfolding by thermal shift, polydispersity by size exclusion chromatography (SEC), and purity by SDS-PAGE (**Table 1,** fig. S3 and S4). The antibodies all appeared as expected for intact immunoglobulins, with 4A5 exhibiting a slightly delayed SEC retention

volume. All four antibodies exhibited low- to mid- nanomolar equilibrium affinities for the SARS-2 spike (*15*) as measured by BLI. Additional measurements with SARS-2 HexaPro, an ultra-stable SARS-2 spike with a total of six proline mutations relative to wild-type spike (*17*), confirmed these affinities. Finally, for 3A3 Fab binding to the SARS-2 HexaPro S2 domain, the K_d of ~2.5 nM was again consistent by both SPR and BLI and the binding on and off rates in the absence of S1 were found to be ~2×10^6/Ms and 5×10-3/s, respectively (fig. S4).

ELISA was used to assess the ability of these antibodies to bind spike proteins from a variety of coronaviruses (SARS-1, SARS-2, MERS, and HKU1) as well as SARS-2 HexaPro, coated on plates with RSV F-foldon as a control (**Fig. 1A,** fig. S5) and validated with BLI K_d measurements (**Table 1**, fig. S4D). Antibodies 3A3, 4A5 and 4H2 retained strong binding the SARS-1, MERS and MERS S2 spikes but exhibited significantly reduced binding to HKU1 spike and no detectable binding to RSV F-foldon. Specifically, 3A3 exhibited an affinity of 21 nM for SARS-1 and 23 nM for MERS intact spikes. The foldon binding antibody 3E11 showed relatively high binding affinity ~3-6 nM across all spikes and the RSV F-foldon as expected since these proteins all include foldon domains for stabilization.

Antibody 3A3 binds a conformationally-sensitive S2 epitope

To better understand the basis for spike protein recognition, the SARS-2, SARS-2 HexaPro, MERS, and HKU1 spikes were fully denatured and reduced and subjected to western blotting. Quadruplicate blots were incubated with each full-length antibody and binding to spike polypeptide was detected with anti-human-Fc-HRP and chemiluminescent peroxidase substrate (**Fig. 1B**). Antibodies 4A5, 4H2, and 3E11 detected linearized SARS-2, SARS-2 HexaPro, and MERS spike proteins, with undetectable binding to HKU1 spike. In contrast, 3A3 did not bind any spike protein in western blot, indicating that the 3A3 antibody binds a purely conformational epitope, while the other three antibodies recognize epitopes with significant linear components.

To better understand the 3A3 conformational epitope, we evaluated 3A3 binding to fresh versus stressed SARS-2 spike by ELISA (**Fig. 1, C and D**). Soluble SARS-2 spike has low stability, with lower production yields than SARS-1 and MERS, despite sharing the homologous "2P" proline mutations (~0.5 mg/L versus ~6 mg/L and ~20 mg/L, respectively) (*15, 17, 18*), and is sensitive to freeze-thaw stresses. By contrast, SARS-2 HexaPro includes four additional proline substitutions and exhibits resistance to freeze-thaw stresses (*17*). We stressed spike by three freeze/thaw cycles, which produced SDS-PAGE-detectable aggregates in the SARS-2 spike but not HexaPro (fig. S6) and captured spike on antibody-coated ELISA plates. Antibodies 4A5, 4H2, and 3E11 bound fresh and stressed SARS-2 spike proteins similarly, with 4A5 and 4H2 binding stressed spike slightly better (**Fig. 1D**). However, 3A3 bound stressed 2P spike with a ~150-fold worse EC_{50}, while binding of stressed HexaPro was unaffected due to its improved stability, indicating a reduced capacity to bind misfolded and/or aggregated spike.

Antibody 3A3 neutralizes spike in *in vitro* cellular fusion and pseudovirus infection assays

To investigate the abilities of 3A3, 4A5, and 4H2 to impact spike function, we first employed a mammalian cell fusion assay (**Fig. 2**). A CHO cell line expressing wild-type SARS-2 spike and GFP was incubated with ACE2-expressing HEK 293 cells dyed with the red fluorescent Cell Trace Far Red stain. After 24 hours, large syncytia formed with green CHO cell fluorescence overlapping ~70% of red HEK 293 cell fluorescence, indicating fusion of the CHO and HEK 293 membranes in the presence of no antibody (**Fig.**

153 **2A**) or 100 μg/ml irrelevant human IgG1 (**Fig. 2D)**, 4A5 or 4H2 antibodies **(**fig. S7). Minimal fluorescence
154 colocalization occurred if either the CHO cells did not express SARS-2 spike (**Fig. 2B**) or the HEK 293
155 cells did not express ACE2 (**Fig. 2C**). Incubation with 100 μg/ml (**Fig. 2G**) or 10 μg/ml (**Fig. 2F**) of 3A3
156 significantly reduced colocalization to ~50% ($p < 0.0001$). While 1 μg/ml 3A3 had minimal impact on
157 fluorescence colocalization (**Fig. 2E**), analysis of average cell size showed significantly reduced syncytia
158 size in the presence of as little as 1 μg/ml 3A3 (**Fig. 2, H and I**).

159 We next assessed 3A3 neutralization in an *in vitro* pseudovirus neutralization assay. Antibody 3A3 or
160 isotype control was preincubated for one hour with pseudotyped lentivirus expressing either wild-type or
161 D614G SARS-2 spike, both without stabilizing modifications, then added to HEK293 cells expressing
162 ACE2. The pseudovirus induced luciferase expression in infected cells and the extent of infection was
163 tracked over 72 hours (**Fig. 3**). With one hour of preincubation, antibody 3A3 blocked infection of wild-
164 type spike pseudovirus with an IC_{50} of ~25.4 μg/ml (170 nM) and D614G spike pseudovirus with an IC_{50}
165 of ~1.6 μg/ml (11 nM).

166 **The neutralizing 3A3 epitope is located on the S2 hinge**

167 To identify the specific epitope recognized by 3A3, we used hydrogen-deuterium exchange mass
168 spectrometry (HDX). We measured deuterium uptake of the SARS-2 HexaPro spike alone, as well as bound
169 by the 3A3 IgG or 3A3 Fab (**Supplemental Tables 1 & 2**). Complexes were formed with excess antibodies
170 such that the SARS-2 HexaPro spike was ~90% bound in both cases. We tracked 192 unmodified peptides
171 through the deuteration time course (10^1, 10^2, 10^3, and 10^4 s), covering over half of the protein sequence
172 (fig. S8). We did not search for glycosylated peptides as de-glycosylation had a small effect on 3A3 affinity
173 (**Table 1**). Analysis of the raw deuterium uptake in the SARS-2 HexaPro spike alone shows maintenance
174 of the trimer during the HDX reaction. There was relatively low deuterium uptake in the helix at the center
175 of the trimer and high deuterium uptake in the HR1 helix at the trimer's surface (fig. S9).

176 Antibody epitopes are identified by looking at the difference in deuterium uptake between SARS-2 HexaPro
177 spike in the free and antibody-bound states. We defined a significant difference in a change in deuterium
178 uptake greater than 0.2 Da with a p-value less than 0.01 (**Fig. 4, A and B**). The binding of 3A3 IgG caused
179 such a significant decrease to occur in 12 peptides that redundantly span residues 980 to 1006 of the SARS-
180 2 HexaPro spike (**Fig. 4C** and fig. S10A). These peptides have reduced deuterium uptake with 3A3 IgG at
181 several timepoints during the exchange reaction. An identical result was observed when the 3A3 Fab was
182 used in place of the IgG, consistent with identical binding (**Fig. 4, B and C** and fig. S10B). In contrast to
183 3A3 IgG and Fab, similar experiments with 4A5 and 4H2 antibodies showed no significant difference in
184 deuterium uptake upon antibody addition (fig. S11). The epitopes recognized by 4A5 and 4H2 are distinct
185 from 3A3 and possibly lie in regions where we lack peptides. Taken altogether, these data suggest that the
186 3A3 epitope lies within residues 980 to 1006 of the SARS-2 HexaPro spike.

187 Mapping the difference in deuterium uptake between free and 3A3-bound states onto the structure localizes
188 the epitope to the apex of the S2 domain, distal to the viral envelope (**Fig. 4D**). It covers the end of the HR1
189 helix, the two stabilizing proline mutations (residues 986 and 987), and the CH helix's beginning. This
190 region is highly conserved in sequence and structure across all coronaviruses known to infect humans (**Fig.
191 5, A and B**). The RMSD of Cα atoms ranges from 0.6 Å for HKU1 to 3.1 Å for MERS. To confirm the
192 epitope and show its validity to varied spike proteins, we used BLI to assess 3A3 binding to the MERS S2
193 domain used for selection or a variant with the apex (including the putative epitope residues) replaced by

194 linker sequences. 3A3 strongly bound the MERS S2 domain but lost binding when the apex was deleted
195 (fig. S12). This confirms that 3A3 directly binds the apex of the S2 domain of the spike proteins from varied
196 coronaviruses.

197 **RBD position influences access to the 3A3 epitope**

198 The 3A3 epitope location suggests its accessibility is regulated by the position of the RBDs in the S1
199 domain. The epitope is completely hidden in a closed spike with all three RBDs in the down position and
200 becomes increasingly exposed as one, two, or three of the RBDs adopt an up position or bind the ACE2
201 receptor (**Fig. 5C** and fig. S10C). Consistent with this, 3A3 did not bind a SARS-2 HexaPro spike that was
202 locked into the closed conformation by engineered disulfide bonds (**Fig. 6A, bottom**). However, this
203 constrained spike was recognized by the control 2-4 antibody (**Fig. 6A, top**).

204 We then evaluated 3A3 binding to naturally occurring spike variants with different open versus closed
205 propensities using flow cytometry. We compared the wild-type versus D614G SARS-2 variants observed
206 in the closed state in ~90% versus 5% of particles, respectively (*2, 19*). We observed minimal 3A3 binding
207 to wild-type spike expressed on the surface of mammalian cells after one hour of staining. In contrast, 3A3
208 strongly bound surface-expressed D614G spike (**Fig. 6B**), consistent with this variant providing more
209 frequent access to the 3A3 epitope. Notably, the SARS-2 variants used in this assay did not contain the
210 stabilizing 2P mutations. This shows that 3A3 recognizes an epitope without these two proline mutations
211 present.

212 In the same flow cytometry assay, antibody CR3022 (*20*), a rare SARS-1/ SARS-2 cross-reactive RBD-
213 binding antibody that binds a cryptic epitope requiring RBDs up (*3*), exhibited reduced binding to D614G
214 than wild-type spike (**Fig. 6B**), suggesting it is less relevant than 3A3 for binding a range of circulating
215 SARS-2 strains. Finally, to evaluate the possibility that 3A3 binds immediately following S1 dissociation,
216 capturing the S2 domain in a transient but still prefusion state, we evaluated the binding of 3A3-bound
217 HexaPro to the RBD-binding antibody S309 (*21*), using BLI. Since strong S309 binding was observed, 3A3
218 can bind when at least some S1 monomers are still present (fig. S13).

219 **DISCUSSION**

220 Over the past two decades, the regular emergence of pathogenic coronaviruses motivated our efforts to
221 isolate cross-reactive coronavirus spike antibodies. In all highly pathogenic coronaviruses, the spike protein
222 is responsible for targeting host cells via the S1 domain, which has little sequence similarity across
223 coronaviruses (41-87%; fig. S1). In contrast, the S2 domain mediates viral envelope and target cell
224 membrane fusion through a complex conformational change (*22*), with a correspondingly low tolerance for
225 sequence variation (63-98% similarity; fig. S1). Moreover, neutralizing sera from individuals never exposed
226 to SARS-2 is common in young people and exclusively bind the S2 domain (*22*). Accordingly, S2 is an
227 attractive target for pan-coronavirus antibody therapy and vaccination. With this in mind, we isolated and
228 characterized three highly cross-reactive antibodies binding S2 from a MERS S2 immune phage library.

229 All three antibodies bind SARS-2 HexaPro with low- to mid-nanomolar K_d values (**Table 1**) and exhibit
230 similar binding to HexaPro, SARS-1, SARS-2, and MERS spikes in ELISA assays, with minimal binding
231 to HKU1 spike (**Fig. 1A**). Antibodies 4H2 and 4A5 bind conserved linear epitopes but do not neutralize in
232 cell fusion assays. By contrast, antibody 3A3 binds a conformational epitope conserved across β

coronavirus clades with a 2.5 nM affinity for SARS-2, 21 nM for SARS-1 and 23 nM for MERS intact spikes (**Table 1**). It exhibits selectivity for fresh versus stressed SARS-2 spike (ELISA EC_{50} ~125-fold higher), suggesting 3A3 could be used to monitor spike quality (**Fig. 1C and D**). Moreover, 3A3 binds SARS-2 spike when expressed on the mammalian cell surface and neutralizes in multiple *in vitro* assays (**Fig. 2 and 3**), with greater sensitivity for the more transmissible SARS-2 D614G variant.

The 3A3 binding site was identified by HDX mass spectrometry as a cryptic epitope at the apex of S2 (**Fig. 4**), under the S1 domain. This region is completely obscured by the S1 domain when the RBDs are in the three-down or "closed" conformation but is progressively exposed as the three RBDs transition to one-up, two-up, and finally the three-up, "open" conformation (**Fig. 5C**). Biochemical data are consistent with this analysis, as 3A3 does not readily bind spike variants with RBDs stabilized in the "down" position but does bind those with RBDs stabilized in the "up" position. Cryo-EM images show wild-type SARS-2 spike primarily in the three RBDs down "closed" conformation (*2*) and 3A3 exhibits weak binding to this protein when expressed on the mammalian cell surface (**Fig. 6D**). Similarly, a soluble HexaPro variant with all RBDs constrained in the down position is not bound by 3A3 (**Fig. 6A**). By contrast, stabilized SARS-1 and SARS-2 spikes appear more often with one RBD-up than their wild-type counterparts in cryo-EM images (*2, 23*) and 3A3 binds stabilized SARS-2 spike with ~2.5 nM K_d affinity (**Fig. 1 and Table 1**). The RBDs are even more commonly "up" in the SARS-2 HexaPro ultra-stable and stabilized MERS spikes, which are bound tightly by 3A3: two RBDs are up in ~30.6% of HexaPro images (*17*), while one or two RBDs are up in >90% of MERS images (*18*).

Antibody 3A3 more potently neutralizes the highly transmissible D614G than wild-type SARS-2 spike. The naturally occurring D614G spike now dominates circulating SARS-2 strains, is more stable than wild-type SARS-2 spike, and samples the RBD-up state more frequently (*19*). Consistent with our understanding of this epitope, 3A3 binds D614G more readily than wild-type spike in the absence of receptor, as monitored by flow cytometry (**Fig. 6D**), and more potently neutralizes pseudovirus expressing D614G versus wild-type spike (**Fig. 3**). Although 3A3 cannot readily access its epitope on surface-displayed wild-type spike, its ability to neutralize wild-type spike (**Fig. 3**) indicates that it may bind and trap spike after ACE2 engagement or S1 dissociation exposes the 3A3 epitope but before the spike conformational change.

The 3A3 epitope is highly conserved across human coronaviruses. This epitope has high sequence identity (48%) and similarity (70%, **Fig. 5A**) among seven human coronaviruses. Moreover, 3A3's ability to bind SARS-1, SARS-2 and MERS spikes with similar sensitivities supports the concept that while binding depends on RBD position, it is independent of RBD sequence or receptor specificity. The structure of the 3A3 epitope is highly conserved across wild-type (PBD 6XR8), 2P (PDB 6VSB), HexaPro (PDB 6XKL), stabilized D614G (PDB 6XS6), and non-stabilized D614G (PDB 7KDL) SARS-2 spike with RMSD of ≤0.7 Å, but the efficiency of 3A3 binding is altered for each, indicating that epitope accessibility impacts 3A3 binding affinity. ELISA may weakly detect binding to HKU1 spike because these spikes rarely sample the RBD-up configuration, even in stabilized forms, and the 3A3 epitope is poorly accessible (*24*). Neutralization of other coronavirus spikes by 3A3 requires further investigation.

The location of the 3A3 epitope suggests a spike neutralizing mechanism. The 3A3 epitope is near the "jackknife hinge" on the S2 domain between HR1 and the central helix, converting from a hairpin turn into a long, straight helix. This transition is the key event in spike conformational change; accordingly, the stabilizing "2P" proline substitutions are also located in this region. There are no glycosylation sites to

impede the transition (*25*). The binding of 3A3 to the pre-fusion hairpin region near the trimer epicenter may lock spike in its pre-fusion conformation and prevent movement of the fusion peptide. Confirmation of this presumptive neutralizing mechanism awaits high-resolution structural analysis.

Although S2 targeting antibodies exist, very few S2 specific antibodies have been reported, and even fewer have been described in detail. Chi *et al.* describe over twenty SARS-2 S2 antibodies, several of which are neutralizing but do not discuss their cross-reactive binding, epitopes, or mechanisms of neutralization (*26*). In other work, an anti-S2 antibody was reported to bind the SARS-2 and HKU1 spikes near the S2 base, opposite the 3A3 apex epitope, with weakly neutralizing activity (*27*), and recently a MERS/OC43 binding antibody was reported that binds this same region and neutralizes MERS (*28*). Antibodies neutralizing SARS-1 epitopes at the base of S2 on the HR2 or HR1 peptides were also reported but not fully characterized (*29, 30*).

Therapeutic antibody cocktails may benefit from the inclusion of neutralizing antibodies targeting S2, such as a humanized 3A3, since simultaneous targeting of multiple epitopes can improve protection and reduce the risk of escape variants. For example, antibodies binding the MERS S2 domain are potently neutralizing individually but synergize with antibodies blocking receptor binding and prevent the emergence of viral escape mutants only when used together (*31*). However, SARS-2 cocktails are currently approved or in development focus on the RBD and S1 (*4*). Regeneron's approved therapeutic cocktail REGN-COV2 is a mixture of two noncompeting RBD binding antibodies. SARS-2 spike variants have already been identified to evade both antibodies, one requiring only a single amino acid substitution and another found in a patient after treatment with REGN-COV2 (*32*). The inclusion of neutralizing antibodies targeting S2 in therapeutic cocktails could provide a second layer of defense, targeting an epitope independent of the RBD.

Mapping conserved, especially neutralizing, spike epitopes will help guide the design of broadly protective immunogens able to protect against all highly pathogenic human coronaviruses. This will include spike engineering to reduce some regions' immunodominance while increasing the immunogenicity of conserved epitopes, analogous to prior efforts with the RSV F antigen (*33*). While S2 antibodies are elicited by infection and can be neutralizing and cross-reactive, the vast majority of naturally occurring neutralizing antibodies target the immunodominant RBD (*34*). The S2-binding antibodies described here were generated by direct immunization with stabilized S2, suggesting that immunization with a mixture of spike and isolated S2 may promote the generation of anti-S2 antibodies. The high immunogenicity of the foldon domain, as indicated by the high frequency of foldon-binding scFvs isolated in this work, implies that the foldon may need to be shielded to avoid generating unprotective responses when employed in vaccine antigens.

There are several limitations to this work as currently described. First, a structure showing the atomic details of 3A3 complexed with spike would provide additional insight into the mechanism of binding and neutralization. However, structures of antibodies bound to S2 are generally challenging to obtain with just one structure available of an antibody binding near the HR2 stem (*28*). It is possible that 3A3 binding distorts spike structure, disturbing otherwise ordered regions. Accordingly, additional efforts to better understanding the molecular underpinnings of 3A3/ spike interactions are underway. Second, while we have shown that 3A3 binds spike from all three highly pathogenic coronaviruses with similar affinities, we have only demonstrated its ability to neutralize SARS-2 spikes *in vitro*. Demonstration of broad neutralization in addition to broad recognition would increase the potential relevance of this epitope for

315 future therapeutics. The 3A3 epitope is highly conserved, with pairwise comparisons showing between 56%
316 and 100% identity to the SARS-2 epitope for MERS and SARS-1, respectively (fig. S14). Since 3A3
317 affinity for the least similar MERS spike is comparable to that for the SARS-2 spike and greater than for
318 HKU1, it seems likely that binding and neutralization depend primarily on RBD position epitope
319 accessibility. The most concerning emerging SARS-2 variants have one conservative substitution in this
320 epitope in B.1.1.7, identified in the United Kingdom, and has no changes in this epitope in B.1.351,
321 identified in South Africa (fig. S14).

322 Here we report an antibody binding of the first reported neutralizing S2 epitope, which is conserved across
323 all highly pathogenic coronavirus strains. HD mapping identified the epitope in the hinge at the S2 apex,
324 suggesting 3A3 locks spike in its pre-fusion conformation. This conformationally sensitive epitope
325 suggests that 3A3 could be used as a sensitive reagent to assess spike protein quality in both academic and
326 industrial settings. Interestingly, 3A3 spike binding and pseudovirus neutralization is enhanced for
327 emerging SARS-CoV-2 spike variants with increased transmissibility, apparently because these variants
328 stabilize the RBDs in the up position required for epitope accessibility. Future work will evaluate 3A3
329 neutralization of other coronavirus strains *in vitro* and *in vivo* and high-resolution structural analysis to
330 determine the precise antibody footprint and neutralizing mechanism.

331

332 **MATERIALS AND METHODS**

333 **Experimental Design**

334 This study's objective was to isolate antibodies with broad cross-reactivity to spike S2 domains and
335 characterize the neutralizing epitopes identified. Mice were immunized with stabilized MERS S2 and their
336 antibody repertoires were captured in a phage display library. After panning against MERS S2 and full-
337 length SARS-2 spike, three antibodies, 3A3, 4A5 and 4H2, were isolated and biophysically characterized.
338 The three antibodies were evaluated in mammalian cell fusion assays, where only 3A3 inhibited the fusion
339 of cells expressing SARS-2 spike with cells expressing the ACE2 receptor. The neutralization potency of
340 3A3 in a pseudotyped lentiviral assay was assessed for both wild-type and D614G SARS-2 spike. Finally,
341 HDX mass spectroscopy was used to locate the epitope of 3A3 at the apex of S2, with confirmatory
342 experiments performed by BLI and flow cytometry.

343 **Spike Expression**

344 Soluble coronavirus spikes and spike variants were expressed and purified as previously described **(*15, 17*)**.
345 SARS-2 **(*15*)**, SARS-1 (*23*), and HexaPro **(*17*)** spikes were expressed in ExpiCHO cells (ThermoFisher
346 Scientific). MERS **(*18*)**, HKU1 (*18*), and the SARS-2 variants HexaPro S2 (residues 697-1208 of the SARS-
347 2 spike with an artificial signal peptide, proline substitutions at positions 817, 892, 899, 942, 986 and 987
348 and a C-terminal T4 fibritin domain, HRV3C cleavage site, 8xHisTag and TwinStrepTag), HexaPro RBD-
349 locked-down (HexaPro with S383C-D985C substitutions), and aglycosylated HexaPro (HexaPro treated
350 with Endo H overnight at 4 °C leaving only one N-acetylglucosamine attached to N-glycosylation site) as
351 well as MERS S2-only (residues 763-1291 of MERS-2P with 8 additional stabilizing substitutions), MERS
352 S2-apex-less (MERS S2-only construct with residues 811-824 replaced with GGSGGS and residues 1042-
353 1073 replaced with a flexible linker) were expressed in Freestyle 293-F cells (ThermoFisher Scientific).

354 **Murine immunization**

355 Three BALB/c mice were immunized subcutaneously with 5μg pre-fusion stabilized MERS S2 and 20 μg
356 of ODN1826 + 100 μl of 2X Sigma Adjuvant System (SAS; Sigma) containing monophosphoryl lipid A
357 and trehalose dimycolate in squalene oil. Four weeks later, the mice were boosted with the same dose of
358 the same mixture. Three weeks after boosting, the mice were sacrificed and spleens were collected in
359 RNALater (ThermoFisher). The University approved mouse protocols of Texas at Austin IACUC (AUP-
360 2018-00092).

361 **Phage display antibody library construction**

362 RNA was isolated from the aqueous phase of homogenized spleens mixed with 1-bromo-3-chloropropane
363 and purified with the PureLink RNA kit (Invitrogen) separately. The Superscript IV kit (Invitrogen) was
364 used to synthesize cDNA. The V_H and V_L sequences from each immunized mouse were amplified with
365 mouse-specific primers described by Krebber *et al.* (*13*). Maintaining separate reactions for each mouse,
366 the V_L and V_H regions were joined by overlap extension PCR for each immunized mouse spleen to generate
367 VL-linker-VH fragments (scFv) which the linker region encodes the amino acids $(Gly_4Ser)_4$ and *Sfi*I sites
368 flanked the scFv sequence. The scFv PCR products were pooled cloned into pMopac24 (*14*) via *Sfi*I cut
369 sites to encode the M13 phage pIII protein fused to an scFv with a c-terminal myc tag. This library was
370 then transformed to XL1-Blue (Agilent Technologies) *E. coli*. The total number of transformants was 3.1
371 $\times 10^8$ with <0.01% background based on plating.

372 **Phage display and panning**

373 The *E.coli* containing the library were expanded in growth media (2×YT with 1% glucose, 200 μg/mL
374 ampicillin, 10 μg/mL tetracycline) at 37 °C to an OD_{600} of 0.5, then infected with 1×10^{11} pfu/ml M13K07
375 helper phage (NEB) and induced with 1mM isopropyl β-d-1-thiogalactopyranoside. After two hours of
376 shaking at room temperature, 12.5 μg/ml of kanamycin was added for phage expression overnight. Phage
377 were precipitated in 20% PEG-8000 in 2.5 M NaCl, titered by infection of XL1-Blue and plating, and used
378 for Round 1 panning. This process was repeated for each round of panning, starting from overnight growth
379 of the output phage from each round.

380 Four rounds of panning were used to isolate scFvs binding both MERS S2 and SARS-2 spike using the
381 following solutions coated on high binding plates: 2 μg/ml anti-c-myc tag antibody (Invitrogen) to eliminate
382 phage expressing no or truncated scFv (Round 1), 2 μg/ml MERS S2 (Round 2), 2 μg/ml SARS-2 spike
383 (Round 3), and 0.4 μg/ml SARS-2 spike (Round 4). In each round of panning, the plates were blocked with
384 5% non-fat milk in phosphate-buffered saline (PBS) with 0.05% Tween-20 (PBS-T), and phage were
385 preincubated with 5% non-fat milk in PBS-T for 30 minutes before incubation on the plate for 1.5 hours at
386 room temperature. After thorough washing with PBS-T, output phage was eluted using 0.1 M HCl at pH
387 2.2, neutralized with ~1:20 2M Tris base, and allowed to infect XL1-Blue cells overnight amplification.

388 Random clones isolated after Round 3 and Round 4 of panning were sequenced and unique clones were
389 tested by monoclonal phage enzyme-linked immunosorbent assay (ELISA) on plates coated with SARS-2
390 spike or RSV F foldon at 2 μg/ml in PBS. Briefly, plates were coated overnight at 4°C, washed with PBS-
391 T, then blocked with PBS-T and 5% milk. Phage were allowed to bind for one hour at room temperature,
392 thoroughly washed with PBS-T, then incubated with 1:2000 anti-M13 pVIII-HRP (GE Healthcare) in PBS-

393 T 5% milk for another hour. After washing, the plate was developed with the TMB Substrate Kit (Thermo
394 Scientific), quenched with an equal volume of 1 M HCl and evaluated by absorbance at 450 nm (fig. S2).

395 **Antibody expression, purification, and quality control**

396 Full-length antibody versions of 3A3, 4A5, 4H2, and 3E11 were cloned as previously described (*35*) as
397 mouse variable region-human IgG1 constant region chimeras. Antibodies were expressed in ExpiCHO
398 (ThermoFisher Scientific) cells according to the high titer protocol provided and purified on a Protein A
399 HiTrap column (GE Healthcare) with the ACTA Pure FPLC system (GE Healthcare), and buffer exchanged
400 to PBS. SDS-PAGE analyzed each purified antibody (3 µg antibody per well) under reducing and non-
401 reducing conditions (fig. S3A) and by analytical size exclusion chromatography on a Superdex S200
402 column (GE Healthcare) (fig. S3B).

403 Mouse Fab fragments of each sequence were generated by cloning the V_H and V_L regions upstream of heavy
404 chain constant regions with a 3C protease site in the hinge (*18*) and a mouse kappa chain, respectively.
405 After expression, protein A purified protein was digested with human rhinovirus 3C protease, and the flow-
406 through from a protein A HiTrap column was collected. Excess 3C protease was removed by incubation
407 with Ni Sepharose 6Fast Flow beads (GE Healthcare). Fully murine antibodies were produced by cloning
408 the VH regions into a mouse IgG2 expression cassette in the pAbVec background, co-transfected with the
409 appropriate mouse IgK plasmid (*36*), and purified as described above.

410 According to the kit instructions, the thermal unfolding temperatures of the chimeric antibodies (0.3 mg/ml)
411 were assessed in triplicate using the Protein Thermal Shift Dye Kit (ThermoFisher Scientific). Continuous
412 fluorescence measurements (λ_{ex} = 580 nm, λ_{em} = 623 nm) were performed using a ThermoFisher ViiA 7
413 Real-Time PCR System, with a temperature ramp rate of 0.05°C/sec increasing from 25°C to 99°C (fig. S3,
414 C and D).

415 **ELISA evaluation of antibody cross-reactivity and binding to stressed spike**

416 ELISAs were performed as described above throughout the work. For testing each antibody's specificity,
417 plates were coated with 1 µg/ml of purified spike proteins (SARS-1, SARS-2, SARS-2 HexaPro, MERS,
418 HKU1, and RSV F foldon) in PBS. Duplicate serial dilutions of each full-length antibody were allowed to
419 bind each coat, and the secondary antibody solution was a 1:1200 dilution of goat-anti-human IgG Fc-HRP
420 (SouthernBiotech). ELISA curves were fit to a 4-parameter logistic curve (**Fig. 1A**).

421 To stress the spike proteins, fresh aliquots of SARS-2 and SARS-2 HexaPro spikes were thawed and split.
422 One half of the aliquot was stressed by incubation at -20°C for 5 min, then 50°C for 2 min for a total of
423 three temperature cycles. The freshly thawed and stressed spikes were serially diluted and captured on
424 ELISA plates coated with each full-length antibody at 1 µg/ml or nothing (no coat). The ELISA was carried
425 out as above with 3% w/v BSA in place of milk in the diluent and blocking buffer and Strep-Tactin-HRP
426 (IBA) as the secondary reagent (**Fig. 1, C and D**). For each fresh and stressed spike, 8 µg was analyzed by
427 SDS-PAGE under non-reducing conditions (fig. S3).

428 **Western blot of antibody binding to coronavirus spike proteins**

429 Purified coronavirus spike proteins (SARS-2 HexaPro, SARS-2, MERS, and HKU1) were reduced and
430 boiled, and 50 ng of each was subjected to SDS-PAGE and transfer to PVDF membranes in quadruplicate.
431 After blocking with PBS-T with 5% milk, the membranes were probed with 0.2 µg/ml 3A3, 1 µg/ml 4A5,
432 1 µg/ml 4H2 or 0.2 µg/ml 3E11 for 1 hour at room temperature. After washing with PBST, the membranes
433 were incubated with 1:4000 goat anti-human IgG Fc-HRP for 45 minutes at room temperature, then
434 developed with the SuperSignal West Pico Chemiluminescent Substrate (Thermo Scientific) and imaged
435 (**Fig. 1B**).

436 **Surface plasmon resonance and biolayer interferometry (BLI) measurements**

437 SPR was used to determine the binding kinetics and affinity of the 3A3 Fab and HexaPro S2 interaction.
438 An anti-StrepTagII Fab was covalently coupled to a CM5 sensor chip, which was then used to capture
439 purified HexaPro S2 by the c-terminal twin StrepTag to ~80 response units (RU) in each cycle using a
440 Biacore X100 (GE Healthcare). The binding surface was regenerated between cycles using 0.1% SDS
441 followed by 10 mM Glycine at pH 2. The 3A3 Fab was serially diluted from 12.5 nM to 1.56 nM and
442 injected over the blank reference flow cell and then HexaPro S2-coated flow cell in HBS-P+ buffer. Buffer
443 was also injected through both flow cells as a reference. The data were double-reference subtracted and fit
444 to a 1:1 binding model using BIAevaluation software.

445 To determine the affinity of 3A3 Fab by BLI, anti-human IgG Fc sensors were coated with the anti-foldon
446 antibody identified in this work (3E11) at 20nM in kinetic buffer. MAb coated sensors were then incubated
447 with HexaPro S2 at 60nM until a response of 0.6nm was obtained. Association of 3A3 Fab was recorded
448 for 5 minutes in kinetics buffer, starting at 100nM followed by 1:2 dilutions. Dissociation was recorded for
449 10 minutes in the kinetics buffer. Kd values were obtained using a 1:1 global fit model using the Octet
450 instrument software. 3A3 Fab kinetics measurement was repeated once (fig. S4B).

451 Apparent K_ds of IgGs were measured using the Octet Red96 (ForteBio) instrument. Anti-Human IgG Fc
452 (AHC) (ForteBio) sensors were loaded with mAbs in the kinetic buffer (0.01% BSA and 0.002% Tween-
453 20 in PBS) at 10 nM until a response of 0.6nm was reached. Association curves were recorded for 5-30 min
454 by incubating the sensors in different concentrations of SARS-2 HexaPro, SARS-2, and aglycosylated
455 HexaPro, starting from 100nM and serial 1:2 dilutions. The dissociation step was recorded for 10-20 min
456 in the kinetic buffer. Steady-state K_d values were determined using the response values obtained after five
457 minutes of association using the Octet analysis software (**Table 1** and fig. S4C).
458
459 To compare 3A3 binding to HexaPro and "Down" HexaPro, anti-Human IgG Fc (AHC) (ForteBio) sensors
460 were loaded with 3A3 mAb in kinetic buffer at 10 nM until a response of 0.6nm was reached. After a
461 baseline step, the sensors were briefly incubated with either HexaPro or "Down" HexaPro, both at 60nM.
462 Short dissociation step recorded in the kinetic buffer (**Fig. 6A**).

463 To evaluate 3A3 binding to HexaPro captured by an RBD binder (IgGS309), Anti-Human Fc Sensors were
464 used to pick up IgGS309 (20 nM) to a response of 0.6 nm. Then mAb coated tips were dipped into wells
465 containing HexaPro (50 nM) to a response of 0.6 nm and then dipped into wells containing murine-3A3
466 (50 nM), irrelevant murine mAb (50 nM), or buffer. Association of m3A3/irrelevant mAb was measured

467 for 5 min and dissociation for 10 min. A similar experiment was also performed but in the reverse
468 orientation where anti-mouse Fc sensors were used to pick up murine-3A3 (fig. S13).

469 Octet Red96 (ForteBio) instrument was used. Between every loading step, sensors were washed with
470 kinetics buffer for 1 minute. Before use, sensors were hydrated in the kinetics buffer for 10 minutes. After
471 each assay, the sensors were regenerated using 10mM Glycine, pH1.5.

472 **Confocal cell fusion assay**

473 On day 0, the CHO-T cells (Acyte Biotech) were transfected with either pPyEGFP (*37*), 1:4 pWT-SARS-
474 2-spike:pPyEGFP, and 1:4 pD614G-SARS-2-spike:pPyEGFP using Lipofectamine 2000 (Life
475 Technologies), and media was replaced on day 1. On day 2 after transfection, HEK-293T-hACE2 cells
476 (BEI, NR-52511), which stably expresses human ACE2, were stained with 1 μM CellTrace Far Red dye
477 (Invitrogen, Ex/Em: 630/661 nm) in PBS for 20 minutes at room temperature, then quenched with DMEM
478 with 10% heat-inactivated FBS for 5 minutes, and resuspended in fresh media. CHO-T cells expressing
479 EGFP or EGFP and surface spike were preincubated with the antibody for one hour at 37°C, then mixed
480 with HEK-hACE2 cells at a ratio of 5:1 in 24-well plates with a coverslip on the bottom of each well. On
481 day 3, after 20 hours of coincubation, the coverslip with bound cells was washed once with PBS and fixed
482 with 4% paraformaldehyde for 20 min at room temperature, washed again, and mounted on slides with
483 DAPI-fluoromount-G (Southern Biotech). Images were collected with Zeiss LSM 710 confocal microscope
484 (Carl Zeiss, Inc) and processed using ImageJ software (http://rsbweb.nih.gov/ij) (**Fig. 2** and fig. S7).

485 The cell fusion level was determined by two different statistical analysis methods. The first statistical
486 analysis was based on the percentage of HEK-ACE2 pixels (red) colocalizing with spike expressing CHO
487 pixels (green), which was determined by the following equation within the JACoP plugin for ImageJ (*38*):
488

489 $$\text{HEK} - \text{ACE2 colocalization\%} = \frac{(summed\ intensities\ at\ 633\ nm\ wavelength\ of\ HEK - ACE2\ pixels\ colocalizaing\ with\ CHO\ pixels)}{(summed\ intensities\ at\ 633\ nm\ wavelength\ of\ HEK - ACE2\ pixels)}$$

490

491 The colocalization percentage for each independent image was determined using the Manders' coefficient.
492 The second statistical analysis was based on the average HEK-ACE2 cell size after the coincubation with
493 CHO cells using the ImageJ software. The image of HEK-ACE2 (red fluorescence color at 633 nm
494 wavelength) was converted into 16-bit in greyscale and adjusted the threshold to highlight the cell structure.
495 The average cell size was automatically counted with the "Analyze Particles" tab with a size threshold (50-
496 infinity) to exclude the background noise. The cell on the edge was excluded. The statistical significance
497 of either HEK-ACE2 colocalization percentage or average cell size between different conditions was
498 calculated with ANOVA using GraphPad Prism 7 (GraphPad Software). Values represent the mean and
499 standard deviation of at least 160 cells.
500

501 **Lentiviral plasmids**

502 Plasmids required for lentiviral production were obtained from BEI resources. Plasmids expressing the HIV
503 virion under the CMV promotor (HDM-Hgpm2, pRC-CMV-Rev1b, and HDM-tat1b) were provided under
504 the following catalog numbers NR-52516, NR-52519, and NR-52518, respectively(*39*). Plasmids for
505 lentiviral backbone expressing a luciferase reporter under the CMV promotor followed by an IRES and
506 ZsGreen (pHAGE-CMV-Luc2-IRES-ZsGreen-W) or human ACE2 gene (GenBank ID NM_021804) under
507 an EF1a promoter (pHAGE2-EF1aInt-ACE2-WT) were provided as NR-52520 and NR52516, respectively

508 (*39*). The envelop vector expressing a codon-optimized WT SARS-COV-2 spike protein (Genbank ID
509 NC_045512) under a CMV promoter was obtained from BEI resources (HDM-IDTSpike-fixK, NR-52514)
510 (*39*), while the plasmid expressing VSV-G (vesicular stomatitis virus glycoprotein) was purchased from
511 Cell Biolabs (pCMV-VSV-G, Part No. RV-110). The HDM-IDTSpike-fixK plasmid was employed as a
512 template for site-directed mutagenesis to generate the expression plasmid for the D614G mutant of SARS-
513 COV-2 Spike protein.
514
515 **Generation of HEK293T-ACE2 target cells, stably expressing human ACE2**
516 Lentiviral vector (pHAGE2-EF1aInt-ACE2-WT) expressing human ACE2 under an EF1a promoter was
517 used to transduce HEK293T cells. Clonal selection depended on the susceptibility to infection by the
518 pseudotyped lentiviral particles; selected clones were validated using western blotting.
519
520 **SARS-COV-2 spike-mediated pseudovirus entry assay**
521 HIV particles pseudotyped with wild type or D614G mutant of SARS-CoV-2 spike were generated in
522 HEK293T cells. A detailed protocol for generating these particles was reported by Crawford et al. (*39*).
523 HEK293T cells were co-transfected with plasmids for (1) HIV virion-formation proteins (HDM-Hgpm2,
524 pRC-CMV-Rev1b, and HDM-tat1b; (2) lentiviral backbone expressing luciferase reporter (pHAGE-CMV-
525 Luc2-IRES-ZsGreen-W), and (3) a plasmid encoding one of the envelope proteins (2019-nCoV Spike-WT,
526 D614G mutant or VSV G as a positive control). 72 hours post-transfection, media containing the
527 pseudovirus particles were collected, filtered, fractionated, and stored at -80 °C. The particles were used
528 directly in cell entry experiments or after pre-incubation with each antibody for one hour at room
529 temperature. After 60–72 hours, a total number of cells per well were estimated using an lncuCyte® ZOOM
530 equipment with a ×10 objective. Then cells were treated with the Bright-Glo Luciferase Assay reagent
531 (Promega, E2610) to detect a luciferase signal (relative luciferase units or RLU) following the
532 manufacturer's protocol. The percentage of entry was estimated as the ratio of the relative luciferase units
533 recorded in the presence and absence of the tested antibody and a half-maximal inhibitory concentrations
534 (IC_{50}) calculated using a 3-parameter logistic regression equation (GraphPad Prism v9.0) (**Fig. 3**).
535

536 **Hydrogen-Deuterium Exchange Mass Spectrometry**

537 Hydrogen-deuterium exchange was performed on 0.50 μM SARS-2 HexaPro spike protein alone (fig. S8
538 & S9) or in the presence of 0.55 μM 3A3 IgG or Fab (**Fig. 4** and fig. S10), 0.75 μM 4A5, or 0.75 μM 4H2
539 (fig. S11). Complexes were incubated for 10 min at 25°C before exchange in 90% deuterium and 20 mM
540 Tris pD 8.0, 200 mM NaCl. The exchange was quenched after 10^1, 10^2, 10^3 and 10^4 s by mixing samples
541 1:1 with cooled 0.2% (v/v) Formic acid, 200 mM TCEP, 8 M Urea, pH 2.3. Samples were immediately
542 flash-frozen in liquid N_2 and stored at −80°C.

543 Samples were thawed and LC-MS performed using a Waters HDX manager and SYNAPT G2-*Si* Q-Tof.
544 Three or four technical replicates of each sample were analyzed in random order. Samples were digested
545 on-line by *Sus scrofa* Pepsin A (Waters Enzymate^{TM} BEH Pepsin column) at 15°C and peptides trapped on
546 a C18 pre-column (Waters ACQUITY UPLC BEH C18 VanGuard pre-column) at 1°C for 3 min at 100
547 μL/min. Peptides were separated over a C18 column (Waters ACQUITY UPLC BEH C18 column) and
548 eluted with a linear 3-40% (v/v) Acetonitrile gradient for 7 min at 30 uL/min at 1 °C and 0.1% (v/v) Formic
549 Acid as the basic LC buffer.

550 MS data were acquired using positive ion mode and either HDMS or HDMS^E. HDMS^E mode was used to
551 collect both low (6 V) and high (ramping 22-44 V) energy fragmentation data for peptide identification in
552 water-only samples. HDMS mode was used to collect low energy ion data for all deuterated samples. All
553 samples were acquired in resolution mode. The capillary voltage was set to 2.8 kV for the sample sprayer.
554 Desolvation gas was set to 650 L/hour at 175 °C. The source temperature was set to 80°C. Cone and
555 nebulizer gas were flowed at 90 L/hour and 6.5 bar, respectively. The sampling cone and source offset were
556 set to 30 V. Data were acquired at a scan time of 0.4 s with a range of 100-2000 m/z. A mass correction
557 was done using [Glu1]-fibrinopeptide B as a reference mass.

558 Water-only control samples were processed by Protein Lynx Global Server v.3.0.2 with a 'minimum
559 fragment ion matches per peptide' of 3 and allowing methionine oxidation. The low and elevated energy
560 thresholds were 250 and 50 counts, respectively, and the overall intensity threshold was 750 counts. The
561 resulting peptide lists were then used to search data from deuterated samples using DynamX v.3.0. Peptide
562 filters of 0.3 products per amino acid and 1 consecutive product were used. Spectra were manually assessed,
563 and figures were prepared using HD-eXplosion (*40*) and PyMOL (*41*). The HDX data summary table
564 (**Table S1**) and complete data table (**Table S2**) are included.

565 **Flow cytometry**

566 On day 0, Expi-293 cells (ThermoFisher) were mock-transfected or transfected with pWT-SARS-2-spike
567 (BEI NR-52514) or pD614G-SARS-2-spike (generated by site-directed mutagenesis). On day 2, 30nM full-
568 length 3A3 or CR3022 was added to ~5×10^5 transfected cells for 1 hour on ice. All cells were collected,
569 washed with PBS with 1% FBS, then incubated with 1:100 goat-anti-human Fc-AF647 for one hour on ice.
570 Cells were washed again, then scanned for AF647 (640 nm excitation, 670/30 bandpass emission)
571 fluorescence on a BD Fortessa flow cytometer and analyzed with FlowJo (**Fig. 6B**).

572 **Statistical analyses**

573 The means ± SD were determined for all appropriate data. For the mammalian cell fusion experiments, a
574 one-way analysis of variance (ANOVA) with Tukey's simultaneous test with *P* values was used to
575 determine statistical significance between groups. Welch's t-test was used to determine the significance of
576 deuterium uptake differences.
577

578 **FIGURES AND TABLES**

579

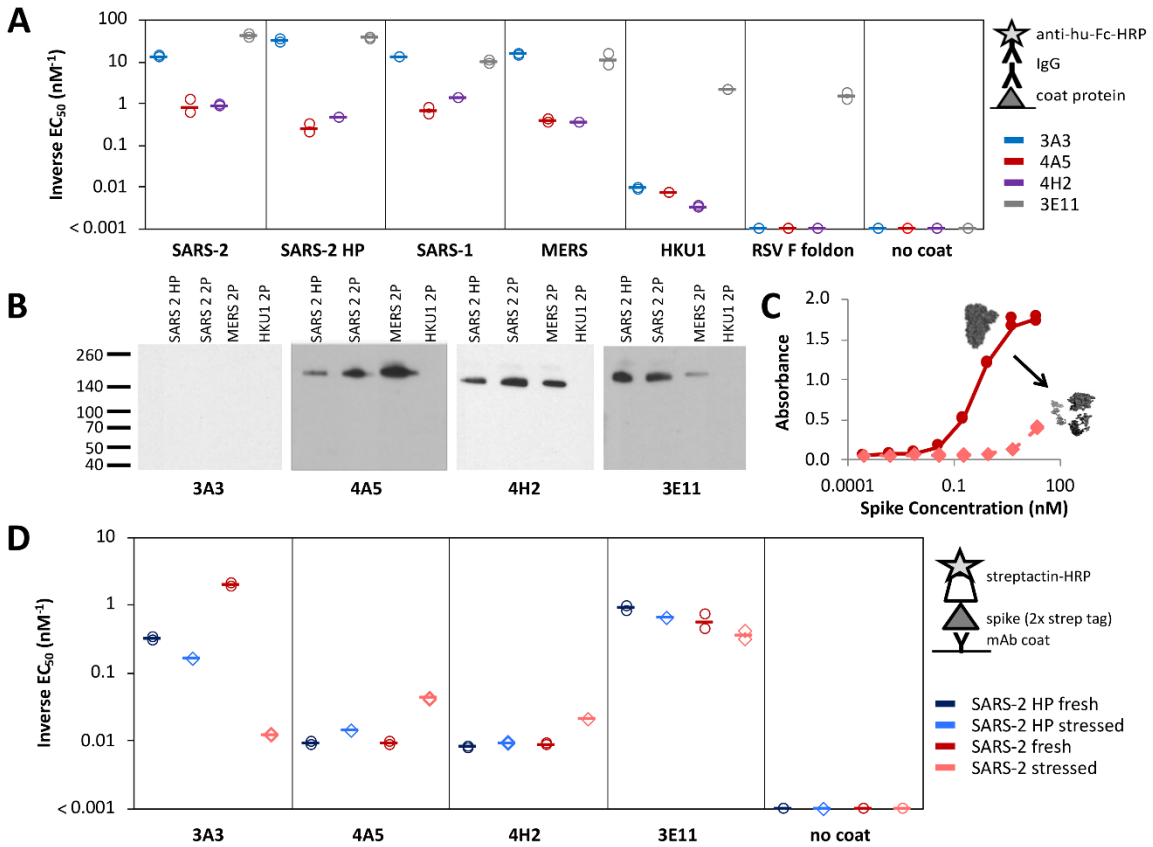

580

581 **Fig. 1. Antibodies 3A3, 4A5, and 4H2 bind to SARS and MERS spike proteins.** (**A**) Full-length 3A3
582 (blue), 4A5 (red), 4H2 (purple), and 3E11 (grey) were tested for binding to plates coated with SARS-2,
583 SARS-2 HexaPro (HP), SARS-1, MERS, HKU1, RSV F foldon, or milk (no coat) proteins by ELISA. (**B**)
584 4A5, 4H2, and 3E11 bind reduced denatured SARS-2 HP, SARS-2, and MERS spike proteins by western
585 blot, but 3A3 does not. No antibodies show binding to HKU1 2P by western blot. The ladder molecular
586 weight is labeled in kDa on the left side. (**C**) ELISA capture of fresh (red circles) or stressed (pink
587 diamonds) SARS-2 spike on 3A3 coated plates. (**D**) Antibodies coated on ELISA plates captured fresh
588 (dark blue or red, circles) or stressed (pink or light blue, diamonds) SARS-2 HP (blue) or SARS-2 (red)
589 spike proteins. For both (**A**) and (**D**), duplicate dilutions of spike over ~5 log in concentration were used to
590 calculate EC_{50} values. For dilution series in which no binding was observed, EC_{50} was assumed to be >1000
591 nM. Open symbols are replicate data and filled rectangles are average data.

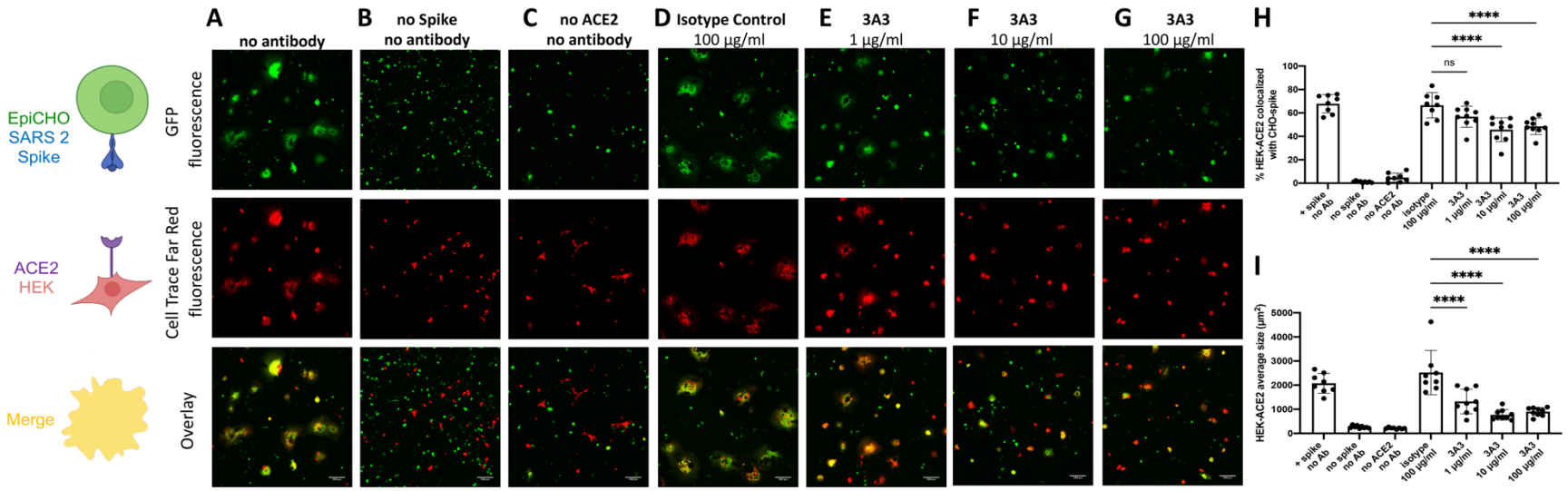

Fig. 2. 3A3 inhibits cellular fusion induced by the interaction of SARS 2 spike with human ACE2. (A) HEK 293 cells stably expressing human ACE2 were stained with Cell Trace Far Red and incubated with a CHO-based cell line transiently expressing wild-type SARS 2 spike and EGFP. The cultures were imaged after 24 hours of incubation for EGFP (green), or Cell Trace Far Red (red) and the level of colocalization (yellow) was evaluated. (**B**) CHO cells not expressing SARS 2 spike and (**C**) HEK 293 cells not expressing ACE2 exhibited minimal fusion. (**D**) When the cultures were preincubated with an irrelevant isotype control antibody, extensive fusion and syncytia formation equivalent to no antibody was apparent. Incubation at (**E**) 1 (7 nM), (**F**) 10 (70 nM), and (**G**) 100 µg/ml (700 nM) 3A3 reduced fusion in a dose-dependent manner with significance reached at 10 µg/ml. (**H**) The percentage of HEK-ACE2 pixels (red) colocalizing with spike expressing CHO pixels (green) was analyzed with the JACoP plugin for ImageJ. Shown are the mean and standard deviation of at least 160 cells per condition from 8-9 independent images. The statistical analysis of colocalization percentages under different conditions were performed with ANOVA. (**I**) The same images per condition used in (**H**) were analyzed for the average cell size of fused HEK-ACE2 with ImageJ as a second statistic method to test the cell fusion level. Shown are the mean and standard deviation. The statistical analysis of average cell sizes under different conditions were performed with ANOVA. The results shown are representative of four independent experiments; **** $p<0.0001$. Scale bar, 100 µm.

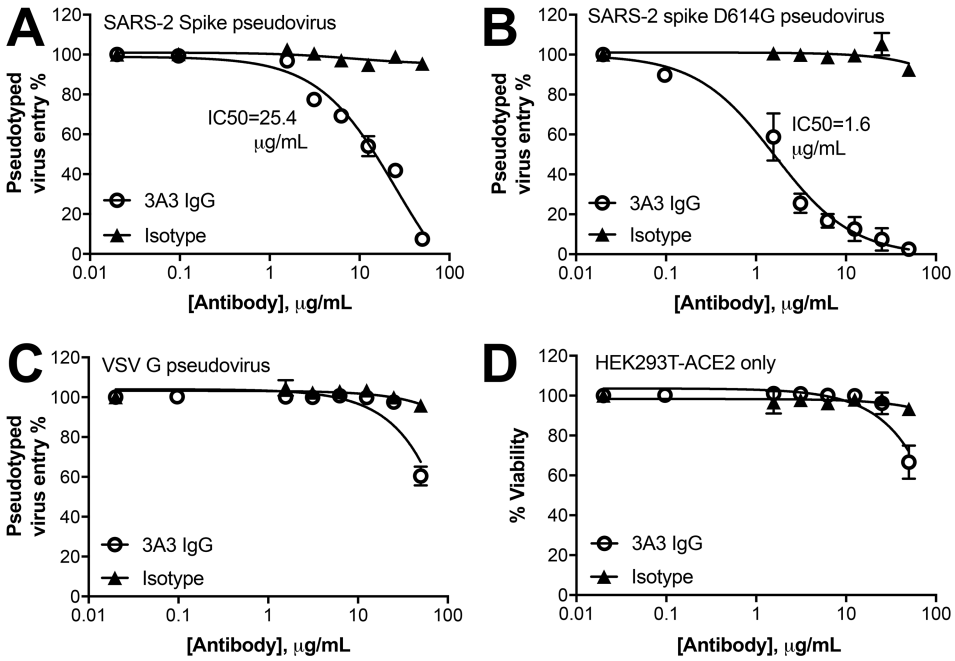

Fig. 3. Effect of the antibody on SARS-CoV-2 entry into HEK293T-ACE2 target cells. Neutralization assays with HIV particles pseudotyped with (**A**) SARS-CoV-2 WT-spike (**B)** SARS-CoV-2 spike D614G mutant and (**C**) VSV-Glycoprotein. The pseudoviruses were incubated with different doses of each antibody for 1 hour at room temperature before adding to HEK293T cells stably expressing ACE2. Viral entry was detected by luciferase luminescence 60-72 hrs later. The entry efficiency of SARS-CoV-2 pseudoviruses without any treatment was considered 100%. **(D)** The effect of the 3A3 antibody and an isotype control on cell proliferation in the absence of pseudovirus. Experiments were performed in triplicate; error bars represent ±SD (n = 3).

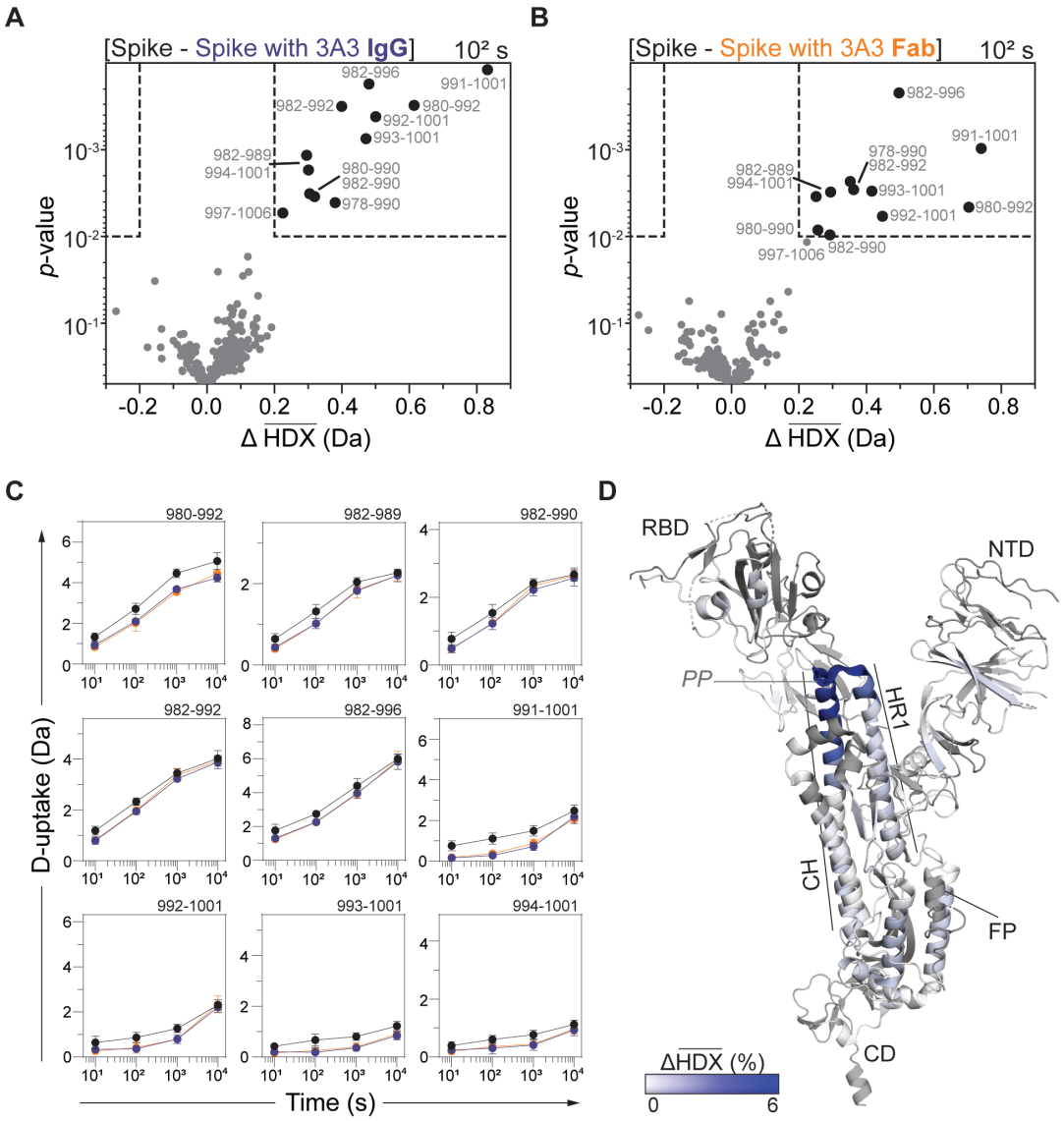

Fig. 4. The 3A3 epitope is located at the apex of the S2 domain. Volcano plots showing changes in deuterium uptake in SARS-2 HexaPro spike peptides upon addition of 3A3 IgG (**A**) or Fab (**B**) after 10^2 s exchange. Significance cutoffs are an average change in deuterium uptake greater than 0.2 Da and a *p*-value less than 10^{-2} in a Welch's t-test (hatched box). Peptides with a significant decrease in deuterium uptake are indicated by black dots and their boundaries labeled. (**C**) Deuterium uptake plots for peptides with a significant decrease in deuterium uptake upon addition of 3A3 (see also fig. S10A). Traces are SARS-2 HexaPro spike alone (black), with 3A3 IgG (blue), and with 3A3 Fab (orange). Error bars are ±2σ from 3 or 4 technical replicates. Y-axis is 70% of max deuterium uptake assuming the N-terminal residue undergoes complete back-exchange. Data have not been corrected for back-exchange. (**D**) Monomeric SARS-2 2P spike (PDB: 6VSB chain B) colored according to the difference in deuterium fractional uptake between SARS-2 HexaPro spike alone and with 3A3 IgG. The figure was prepared using DynamX per residue output without statistics and Pymol. Residues lacking coverage are indicated in grey. Structural features are labeled, including the 2P mutations at residues 986 and 987 (shown as sticks).

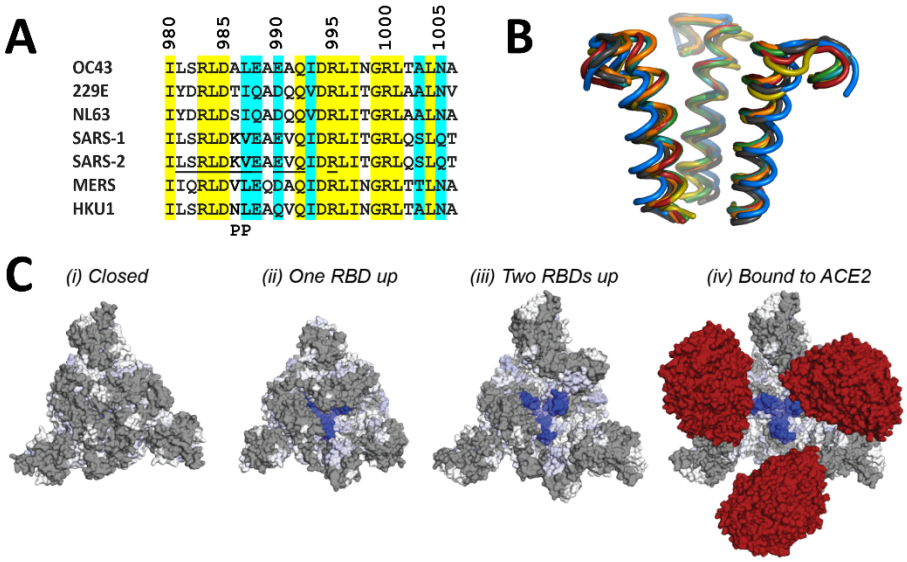

Fig. 5. Structural location of 3A3 epitope and implications for antibody binding. The 3A3 epitope identified by HDX mass spectrometry (SARS-2 amino acids 980-1006) is highly conserved across the spike (**A**) sequences and (**B**) structures of coronaviruses known to infect humans. In (**A**), identical residues are highlighted in yellow and similar residues are highlighted in aqua. Solvent exposed residues visible in spike structures with at least one RBD-up are underlined in the SARS-2 sequence. The location of the two proline mutations introduced to 2P variants are shown below the alignment. In (**B**), the structure of each epitope is displayed as follows: SARS-2 (6VSB) – red, SARS-1 (6CRV, RMSD = 0.8 Å) – orange, MERS (5X5C, RMSD = 3.1 Å) – blue, NL63 (7KIP, RMSD = 2.6 Å) – grey, HKU1 (5I08, RMSD = 0.5 Å) – teal, OC43 (6OHW, RMSD = 0.6 Å) – green, 229E (6U7H, RMSD = 2.0 Å) – yellow. (**C**) Trimeric SARS-2 spike in various conformations colored according to the difference in deuterium fractional uptake between SARS-2 HexaPro spike alone and with 3A3 IgG (as in Figure 4D). The 3A3 epitope (dark blue) within S2 is completely hidden by S1 in the structure of wild-type SARS-2 spike in the (i) three RBDs down or closed conformation (PDB: 6XR8). In structures of stabilized spike with (ii) one RBD-up (PDB: 6VSB), (iii) two RBDs up (PDB: 7A93), or (iv) three RBDs up and bound to ACE2 (red) (PDB: 7A98), the 3A3 epitope is increasingly accessible. Residues lacking coverage in the HDX experiment are indicated in grey. The side view is shown in fig. S10C.

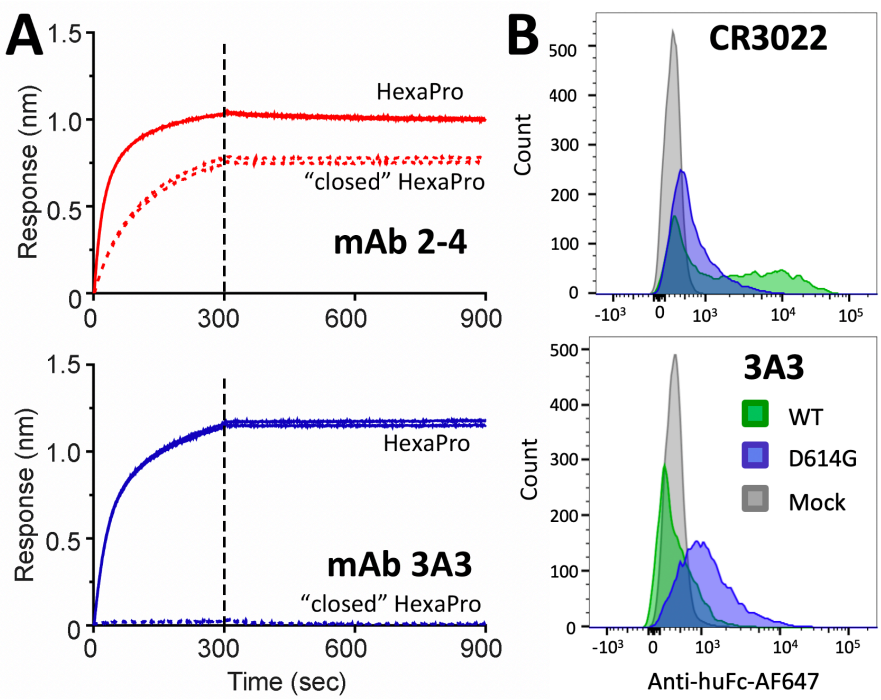

Fig. 6. The 3A3 epitope is inaccessible in the closed conformation of the SARS-2 spike. (**A**) By BLI, the control antibody 2-4 (*42*) (red lines) bound both HexaPro (solid) and HexaPro locked into the "closed" conformation (dashed). 3A3 (blue lines) was able to capture SARS-2 HexaPro (solid), but not "closed" HexaPro. Vertical dashed lines indicate the start of the dissociation phase; paired lines represent data and a fitted curve. (**B**) Antibody 3A3 weakly stains wild-type spike (WT; green) expressing Expi293 cells and more strongly binds D614G spike (blue) expressing cells in flow cytometry. Control Expi293 cells not expressing spike (mock) are shown in grey.

655 **Table 1. Antibody binding affinities for spike variants†**

	Spike variant K_d (nM)						
	SARS-2	**HexaPro S2**	**HexaPro**	**HexaPro aglyc**	**SARS-1**	**MERS**	**MERS S2**
3A3	2.5 ± 0.1	3.2 ± 0.3	12.0 ± 0.3	8.4 ± 0.3	21±0.8	23±1.2	5.9±0.6
4A5	14 ± 2	11.0 ± 0.1	3.2 ± 0.3	10 ± 2	4±0.9	ND	ND
4H2	26 ± 2	63 ± 7	6.4 ± 0.6	9 ± 2	20±2	ND	ND
3E11	5.0 ± 0.2	10 ± 1	3.1 ± 0.3	11 ± 2	5.7±0.5	ND	ND

656 † K_d values are equilibrium affinity of immobilized full-length IgGs on anti-Fc sensors capturing the
657 indicated SARS-2 spike or spike domain, with standard error. All fits had R^2>0.90.
658 ND = no data.
659

660 **REFERENCES**

661 1. Z. Abdelrahman, M. Li, X. Wang, Comparative Review of SARS-CoV-2, SARS-CoV, MERS-CoV, and
662 Influenza A Respiratory Viruses. *Front Immunol* **11**, 552909 (2020).
663 2. Y. Cai, J. Zhang, T. Xiao, H. Peng, S. M. Sterling, R. M. Walsh, Jr., S. Rawson, S. Rits-Volloch, B.
664 Chen, Distinct conformational states of SARS-CoV-2 spike protein. *Science* **369**, 1586-1592
665 (2020).
666 3. M. Yuan, H. Liu, N. C. Wu, I. A. Wilson, Recognition of the SARS-CoV-2 receptor binding domain
667 by neutralizing antibodies. *Biochem Biophys Res Commun*, (2020).
668 4. A. Renn, Y. Fu, X. Hu, M. D. Hall, A. Simeonov, Fruitful Neutralizing Antibody Pipeline Brings
669 Hope To Defeat SARS-Cov-2. *Trends Pharmacol Sci* **41**, 815-829 (2020).
670 5. H. Lv, N. C. Wu, O. T. Tsang, M. Yuan, R. Perera, W. S. Leung, R. T. Y. So, J. M. C. Chan, G. K. Yip,
671 T. S. H. Chik, Y. Wang, C. Y. C. Choi, Y. Lin, W. W. Ng, J. Zhao, L. L. M. Poon, J. S. M. Peiris, I. A.
672 Wilson, C. K. P. Mok, Cross-reactive Antibody Response between SARS-CoV-2 and SARS-CoV
673 Infections. *Cell Rep* **31**, 107725 (2020).
674 6. C. G. Rappazzo, L. V. Tse, C. I. Kaku, D. Wrapp, M. Sakharkar, D. Huang, L. M. Deveau, T. J.
675 Yockachonis, A. S. Herbert, M. B. Battles, C. M. O'Brien, M. E. Brown, J. C. Geoghegan, J. Belk, L.
676 Peng, L. Yang, Y. Hou, T. D. Scobey, D. R. Burton, D. Nemazee, J. M. Dye, J. E. Voss, B. M. Gunn, J.
677 S. McLellan, R. S. Baric, L. E. Gralinski, L. M. Walker, Broad and potent activity against SARS-like
678 viruses by an engineered human monoclonal antibody. *Science*, (2021).
679 7. A. Impagliazzo, F. Milder, H. Kuipers, M. V. Wagner, X. Zhu, R. M. Hoffman, R. van Meersbergen,
680 J. Huizingh, P. Wanningen, J. Verspuij, M. de Man, Z. Ding, A. Apetri, B. Kukrer, E. Sneekes-
681 Vriese, D. Tomkiewicz, N. S. Laursen, P. S. Lee, A. Zakrzewska, L. Dekking, J. Tolboom, L. Tettero,
682 S. van Meerten, W. Yu, W. Koudstaal, J. Goudsmit, A. B. Ward, W. Meijberg, I. A. Wilson, K.
683 Radosevic, A stable trimeric influenza hemagglutinin stem as a broadly protective immunogen.
684 *Science* **349**, 1301-1306 (2015).
685 8. D. Corti, E. Cameroni, B. Guarino, N. L. Kallewaard, Q. Zhu, A. Lanzavecchia, Tackling influenza
686 with broadly neutralizing antibodies. *Curr Opin Virol* **24**, 60-69 (2017).
687 9. R. Channappanavar, L. Lu, S. Xia, L. Du, D. K. Meyerholz, S. Perlman, S. Jiang, Protective Effect of
688 Intranasal Regimens Containing Peptidic Middle East Respiratory Syndrome Coronavirus Fusion
689 Inhibitor Against MERS-CoV Infection. *J Infect Dis* **212**, 1894-1903 (2015).
690 10. L. Lu, Q. Liu, Y. Zhu, K. H. Chan, L. Qin, Y. Li, Q. Wang, J. F. Chan, L. Du, F. Yu, C. Ma, S. Ye, K. Y.
691 Yuen, R. Zhang, S. Jiang, Structure-based discovery of Middle East respiratory syndrome
692 coronavirus fusion inhibitor. *Nature communications* **5**, 3067 (2014).
693 11. C. M. Poh, G. Carissimo, B. Wang, S. N. Amrun, C. Y. Lee, R. S. Chee, S. W. Fong, N. K. Yeo, W. H.
694 Lee, A. Torres-Ruesta, Y. S. Leo, M. I. Chen, S. Y. Tan, L. Y. A. Chai, S. Kalimuddin, S. S. G. Kheng,
695 S. Y. Thien, B. E. Young, D. C. Lye, B. J. Hanson, C. I. Wang, L. Renia, L. F. P. Ng, Two linear
696 epitopes on the SARS-CoV-2 spike protein that elicit neutralising antibodies in COVID-19
697 patients. *Nat Commun* **11**, 2806 (2020).
698 12. Y. Lu, Y. Wang, Z. Zhang, J. Huang, M. Yao, G. Huang, Y. Ge, P. Zhang, H. Huang, Y. Wang, H. Li,
699 W. Wang, Generation of Chicken IgY against SARS-COV-2 Spike Protein and Epitope Mapping. *J*
700 *Immunol Res* **2020**, 9465398 (2020).
701 13. A. Krebber, S. Bornhauser, J. Burmester, A. Honegger, J. Willuda, H. R. Bosshard, A. Pluckthun,
702 Reliable cloning of functional antibody variable domains from hybridomas and spleen cell
703 repertoires employing a reengineered phage display system. *J Immunol Methods* **201**, 35-55
704 (1997).

705 14. A. Hayhurst, S. Happe, R. Mabry, Z. Koch, B. L. Iverson, G. Georgiou, Isolation and expression of
706 recombinant antibody fragments to the biological warfare pathogen Brucella melitensis. *J*
707 *Immunol Methods* **276**, 185-196 (2003).
708 15. D. Wrapp, N. Wang, K. S. Corbett, J. A. Goldsmith, C. L. Hsieh, O. Abiona, B. S. Graham, J. S.
709 McLellan, Cryo-EM structure of the 2019-nCoV spike in the prefusion conformation. *Science* **367**,
710 1260-1263 (2020).
711 16. J. S. McLellan, M. Chen, M. G. Joyce, M. Sastry, G. B. Stewart-Jones, Y. Yang, B. Zhang, L. Chen, S.
712 Srivatsan, A. Zheng, T. Zhou, K. W. Graepel, A. Kumar, S. Moin, J. C. Boyington, G. Y. Chuang, C.
713 Soto, U. Baxa, A. Q. Bakker, H. Spits, T. Beaumont, Z. Zheng, N. Xia, S. Y. Ko, J. P. Todd, S. Rao, B.
714 S. Graham, P. D. Kwong, Structure-based design of a fusion glycoprotein vaccine for respiratory
715 syncytial virus. *Science* **342**, 592-598 (2013).
716 17. C. L. Hsieh, J. A. Goldsmith, J. M. Schaub, A. M. DiVenere, H. C. Kuo, K. Javanmardi, K. C. Le, D.
717 Wrapp, A. G. Lee, Y. Liu, C. W. Chou, P. O. Byrne, C. K. Hjorth, N. V. Johnson, J. Ludes-Meyers, A.
718 W. Nguyen, J. Park, N. Wang, D. Amengor, J. J. Lavinder, G. C. Ippolito, J. A. Maynard, I. J.
719 Finkelstein, J. S. McLellan, Structure-based design of prefusion-stabilized SARS-CoV-2 spikes.
720 *Science* **369**, 1501-1505 (2020).
721 18. J. Pallesen, N. Wang, K. S. Corbett, D. Wrapp, R. N. Kirchdoerfer, H. L. Turner, C. A. Cottrell, M.
722 M. Becker, L. Wang, W. Shi, W. P. Kong, E. L. Andres, A. N. Kettenbach, M. R. Denison, J. D.
723 Chappell, B. S. Graham, A. B. Ward, J. S. McLellan, Immunogenicity and structures of a rationally
724 designed prefusion MERS-CoV spike antigen. *Proc Natl Acad Sci U S A* **114**, E7348-E7357 (2017).
725 19. L. Yurkovetskiy, X. Wang, K. E. Pascal, C. Tomkins-Tinch, T. P. Nyalile, Y. Wang, A. Baum, W. E.
726 Diehl, A. Dauphin, C. Carbone, K. Veinotte, S. B. Egri, S. F. Schaffner, J. E. Lemieux, J. B. Munro, A.
727 Rafique, A. Barve, P. C. Sabeti, C. A. Kyratsous, N. V. Dudkina, K. Shen, J. Luban, Structural and
728 Functional Analysis of the D614G SARS-CoV-2 Spike Protein Variant. *Cell* **183**, 739-751 e738
729 (2020).
730 20. M. Yuan, N. C. Wu, X. Zhu, C. D. Lee, R. T. Y. So, H. Lv, C. K. P. Mok, I. A. Wilson, A highly
731 conserved cryptic epitope in the receptor binding domains of SARS-CoV-2 and SARS-CoV. *Science*
732 **368**, 630-633 (2020).
733 21. D. Pinto, Y. J. Park, M. Beltramello, A. C. Walls, M. A. Tortorici, S. Bianchi, S. Jaconi, K. Culap, F.
734 Zatta, A. De Marco, A. Peter, B. Guarino, R. Spreafico, E. Cameroni, J. B. Case, R. E. Chen, C.
735 Havenar-Daughton, G. Snell, A. Telenti, H. W. Virgin, A. Lanzavecchia, M. S. Diamond, K. Fink, D.
736 Veesler, D. Corti, Cross-neutralization of SARS-CoV-2 by a human monoclonal SARS-CoV
737 antibody. *Nature* **583**, 290-295 (2020).
738 22. K. W. Ng, N. Faulkner, G. H. Cornish, A. Rosa, R. Harvey, S. Hussain, R. Ulferts, C. Earl, A. G.
739 Wrobel, D. J. Benton, C. Roustan, W. Bolland, R. Thompson, A. Agua-Doce, P. Hobson, J. Heaney,
740 H. Rickman, S. Paraskevopoulou, C. F. Houlihan, K. Thomson, E. Sanchez, G. Y. Shin, M. J. Spyer,
741 D. Joshi, N. O'Reilly, P. A. Walker, S. Kjaer, A. Riddell, C. Moore, B. R. Jebson, M. Wilkinson, L. R.
742 Marshall, E. C. Rosser, A. Radziszewska, H. Peckham, C. Ciurtin, L. R. Wedderburn, R. Beale, C.
743 Swanton, S. Gandhi, B. Stockinger, J. McCauley, S. J. Gamblin, L. E. McCoy, P. Cherepanov, E.
744 Nastouli, G. Kassiotis, Preexisting and de novo humoral immunity to SARS-CoV-2 in humans.
745 *Science*, (2020).
746 23. R. N. Kirchdoerfer, N. Wang, J. Pallesen, D. Wrapp, H. L. Turner, C. A. Cottrell, K. S. Corbett, B. S.
747 Graham, J. S. McLellan, A. B. Ward, Stabilized coronavirus spikes are resistant to conformational
748 changes induced by receptor recognition or proteolysis. *Sci Rep* **8**, 15701 (2018).
749 24. A. C. Walls, Y. J. Park, M. A. Tortorici, A. Wall, A. T. McGuire, D. Veesler, Structure, Function, and
750 Antigenicity of the SARS-CoV-2 Spike Glycoprotein. *Cell* **181**, 281-292 e286 (2020).

751 25. Y. Watanabe, Z. T. Berndsen, J. Raghwani, G. E. Seabright, J. D. Allen, O. G. Pybus, J. S. McLellan,
752 I. A. Wilson, T. A. Bowden, A. B. Ward, M. Crispin, Vulnerabilities in coronavirus glycan shields
753 despite extensive glycosylation. *Nat Commun* **11**, 2688 (2020).
754 26. X. Chi, R. Yan, J. Zhang, G. Zhang, Y. Zhang, M. Hao, Z. Zhang, P. Fan, Y. Dong, Y. Yang, Z. Chen, Y.
755 Guo, J. Zhang, Y. Li, X. Song, Y. Chen, L. Xia, L. Fu, L. Hou, J. Xu, C. Yu, J. Li, Q. Zhou, W. Chen, A
756 neutralizing human antibody binds to the N-terminal domain of the Spike protein of SARS-CoV-
757 2. *Science* **369**, 650-655 (2020).
758 27. G. Song, W. T. He, S. Callaghan, F. Anzanello, D. Huang, J. Ricketts, J. L. Torres, N. Beutler, L.
759 Peng, S. Vargas, J. Cassell, M. Parren, L. Yang, C. Ignacio, D. M. Smith, J. E. Voss, D. Nemazee, A.
760 B. Ward, T. Rogers, D. R. Burton, R. Andrabi, Cross-reactive serum and memory B cell responses
761 to spike protein in SARS-CoV-2 and endemic coronavirus infection. *bioRxiv*, (2020).
762 28. M. M. Sauer, M. A. Tortorici, Y.-J. Park, A. C. Walls, L. Homad, O. Acton, J. Bowen, C. Wang, X.
763 Xiong, W. de van der Schueren, J. Quispe, B. G. Hoffstrom, B.-J. Bosch, A. T. McGuire, D. Veesler,
764 Structural basis for broad coronavirus neutralization. *bioRxiv*, 2020.2012.2029.424482 (2020).
765 29. K. M. Lip, S. Shen, X. Yang, C. T. Keng, A. Zhang, H. L. Oh, Z. H. Li, L. A. Hwang, C. F. Chou, B. C.
766 Fielding, T. H. Tan, J. Mayrhofer, F. G. Falkner, J. Fu, S. G. Lim, W. Hong, Y. J. Tan, Monoclonal
767 antibodies targeting the HR2 domain and the region immediately upstream of the HR2 of the S
768 protein neutralize in vitro infection of severe acute respiratory syndrome coronavirus. *J Virol* **80**,
769 941-950 (2006).
770 30. H. A. Elshabrawy, M. M. Coughlin, S. C. Baker, B. S. Prabhakar, Human monoclonal antibodies
771 against highly conserved HR1 and HR2 domains of the SARS-CoV spike protein are more broadly
772 neutralizing. *PLoS One* **7**, e50366 (2012).
773 31. L. Wang, W. Shi, J. D. Chappell, M. G. Joyce, Y. Zhang, M. Kanekiyo, M. M. Becker, N. van
774 Doremalen, R. Fischer, N. Wang, K. S. Corbett, M. Choe, R. D. Mason, J. G. Van Galen, T. Zhou, K.
775 O. Saunders, K. M. Tatti, L. M. Haynes, P. D. Kwong, K. Modjarrad, W. P. Kong, J. S. McLellan, M.
776 R. Denison, V. J. Munster, J. R. Mascola, B. S. Graham, Importance of Neutralizing Monoclonal
777 Antibodies Targeting Multiple Antigenic Sites on the Middle East Respiratory Syndrome
778 Coronavirus Spike Glycoprotein To Avoid Neutralization Escape. *J Virol* **92**, (2018).
779 32. T. N. Starr, A. J. Greaney, A. Addetia, W. W. Hannon, M. C. Choudhary, A. S. Dingens, J. Z. Li, J. D.
780 Bloom, Prospective mapping of viral mutations that escape antibodies used to treat COVID-19.
781 *bioRxiv*, 2020.2011.2030.405472 (2020).
782 33. M. C. Crank, T. J. Ruckwardt, M. Chen, K. M. Morabito, E. Phung, P. J. Costner, L. A. Holman, S. P.
783 Hickman, N. M. Berkowitz, I. J. Gordon, G. V. Yamshchikov, M. R. Gaudinski, A. Kumar, L. A.
784 Chang, S. M. Moin, J. P. Hill, A. T. DiPiazza, R. M. Schwartz, L. Kueltzo, J. W. Cooper, P. Chen, J. A.
785 Stein, K. Carlton, J. G. Gall, M. C. Nason, P. D. Kwong, G. L. Chen, J. R. Mascola, J. S. McLellan, J.
786 E. Ledgerwood, B. S. Graham, V. R. C. S. Team, A proof of concept for structure-based vaccine
787 design targeting RSV in humans. *Science* **365**, 505-509 (2019).
788 34. S. J. Zost, P. Gilchuk, R. E. Chen, J. B. Case, J. X. Reidy, A. Trivette, R. S. Nargi, R. E. Sutton, N.
789 Suryadevara, E. C. Chen, E. Binshtein, S. Shrihari, M. Ostrowski, H. Y. Chu, J. E. Didier, K. W.
790 MacRenaris, T. Jones, S. Day, L. Myers, F. Eun-Hyung Lee, D. C. Nguyen, I. Sanz, D. R. Martinez, P.
791 W. Rothlauf, L. M. Bloyet, S. P. J. Whelan, R. S. Baric, L. B. Thackray, M. S. Diamond, R. H.
792 Carnahan, J. E. Crowe, Jr., Rapid isolation and profiling of a diverse panel of human monoclonal
793 antibodies targeting the SARS-CoV-2 spike protein. *Nat Med* **26**, 1422-1427 (2020).
794 35. A. W. Nguyen, E. K. Wagner, J. R. Laber, L. L. Goodfield, W. E. Smallridge, E. T. Harvill, J. F. Papin,
795 R. F. Wolf, E. A. Padlan, A. Bristol, M. Kaleko, J. A. Maynard, A cocktail of humanized anti-
796 pertussis toxin antibodies limits disease in murine and baboon models of whooping cough. *Sci*
797 *Transl Med* **7**, 316ra195 (2015).

36. E. K. Wagner, A. N. Qerqez, C. A. Stevens, A. W. Nguyen, G. Delidakis, J. A. Maynard, Human cytomegalovirus-specific T cell receptor engineered for high affinity and soluble expression using mammalian cell display. *J Biol Chem*, (2019).
37. A. W. Nguyen, K. C. Le, J. A. Maynard, Identification of high affinity HER2 binding antibodies using CHO Fab surface display. *Protein Eng Des Sel* **31**, 91-101 (2018).
38. S. Bolte, F. P. Cordelieres, A guided tour into subcellular colocalization analysis in light microscopy. *J Microsc* **224**, 213-232 (2006).
39. K. H. D. Crawford, R. Eguia, A. S. Dingens, A. N. Loes, K. D. Malone, C. R. Wolf, H. Y. Chu, M. A. Tortorici, D. Veesler, M. Murphy, D. Pettie, N. P. King, A. B. Balazs, J. D. Bloom, Protocol and Reagents for Pseudotyping Lentiviral Particles with SARS-CoV-2 Spike Protein for Neutralization Assays. *Viruses* **12**, (2020).
40. N. Zhang, X. Yu, X. Zhang, S. D'Arcy, HD-eXplosion: Visualization of hydrogen-deuterium exchange data as chiclet and volcano plots with statistical filtering. *Bioinformatics*, (2020).
41. W. L. DeLano. (DeLano Scientific, San Carlos, CA, 2002).
42. H. Liu, N. C. Wu, M. Yuan, S. Bangaru, J. L. Torres, T. G. Caniels, J. van Schooten, X. Zhu, C. D. Lee, P. J. M. Brouwer, M. J. van Gils, R. W. Sanders, A. B. Ward, I. A. Wilson, Cross-Neutralization of a SARS-CoV-2 Antibody to a Functionally Conserved Site Is Mediated by Avidity. *Immunity* **53**, 1272-1280 e1275 (2020).

ACKNOWLEDGEMENTS

General: The following reagent was contributed by David Veesler for distribution through BEI Resources, NIAID, NIH: Vector pcDNA3.1(-) containing the SARS-Related Coronavirus 2, Wuhan-Hu-1 Spike Glycoprotein Gene, NR-52420 (*24*). The following reagents were obtained through BEI Resources, NIAID, NIH: Human Embryonic Kidney Cells (HEK-293T) Expressing Human Angiotensin-Converting Enzyme 2, HEK-293T-hACE2 Cell Line, NR-52511; SARS-Related Coronavirus 2, Wuhan-Hu-1 Spike-Pseudotyped Lentiviral Kit, NR-52948 (including NR-52514, NR-52516, NR-52517, NR-51518, and NR-52519); and Vector pHAGE2 Containing the ZsGreen Gene, NR-52520.

The authors would like to thank Eduardo A. Padlan, Gregory C. Ippolito, Jason J. Lavinder, and George Delidakis for useful discussions and advice related to this work.

Funding: This work was supported by NIH grants AI127521 (J.S.M.), GM133751 (S.D.) and AI122753 to (J.A.M.), the Bill & Melinda Gates Foundation INV-017592 (J.S.M. and J.A.M.); Welch Foundation grants F-1767 (J.A.M.) and F-1390 (K.D.); NSF RAPID 2027066 (J.A.M.), NSF GRFP (A.N.Q.). This research was, in part, supported by the UT System Proteomics Network (SD).

Author contributions: Conceptualization, Y.H., A.W.N., C.-L.H., A.N.Q, J.S.M. and J.A.M.; Investigation and visualization, Y.H., A.W.N., C.-L.H., R.S., O.S.O., R.W., T.S.K., L.R.A., A.N.Q., K.C.L., A.L.B., A.M.D., Y.L., A.L., and D.A.; Writing – Original Draft, Y.H., A.W.N, T.S.K., S.D. and J.A.M.; Writing – Reviewing & Editing, Y.H., A.W.N., C.-L.H., R.S., O.S.O., R.W., T.S.K., K.D., S.D., J.S.M and J.A.M.; Supervision, K.D., S.D., J.S.M. and J.A.M.

Competing interests: Y.H., A.W.N., C.-L.H., J.S.M. and J.A.M. are inventors on U.S. patent application no. 63/135,913 ("Cross-reactive antibodies recognizing the coronavirus spike S2 domain"). J.S.M. is an

inventor on U.S. patent application no. 62/412,703 ("Prefusion Coronavirus Spike Proteins and Their Use"). C.-L.H., A.M.D., J.A.M., and J.S.M. are inventors on U.S. patent application no. 63/032,502 ("Engineered Coronavirus Spike (S) Protein and Methods of Use Thereof").

Data and materials availability: Data and antibody sequences will be submitted to the Submit data to the Immune Epitope Database and Analysis Resource (iedb.org) and the Coronavirus Immunotherapy Consortium (covic.lji.org).